STATISTICS, OPTIMIZATION AND INFORMATION COMPUTING
Stat., Optim. Inf. Comput., Vol. **13**, March 2025, pp 1266–1279.
Published online in International Academic Press (www.IAPress.org)

A Sine-Cosine Algorithm Approach for Optimal PV and D-STATCOM Integration in Distribution Systems

Oscar Danilo Montoya [1,*], Carlos Alberto Ramírez-Vanegas [2], Luis Fernando Grisales-Noreña [3]

[1] *Facultad de Ingeniería, Universidad Distrital Francisco José de Caldas, Bogotá D.C. 110121, Colombia*
[2] *Departamento de Matemáticas, Facultad de Ciencias Básicas, Universidad Tecnológica de Pereira, Pereira 660003, Colombia*
[3] *Grupo de Investigación en Alta Tensión-GRALTA, Universidad del Valle, Cali 760015, Colombia*

Abstract This study proposes the use of the sine-cosine algorithm (SCA) to optimize the integration of solar photovoltaic (PV) systems and distribution static compensators (D-STATCOMs) in medium-voltage distribution networks. The SCA is applied to determine the optimal siting and sizing of both PV units and D-STATCOMs, utilizing a hybrid discrete-continuous approach to codify the solutions. A power flow analysis based on the successive approximations method is employed to assess system performance, considering voltage regulation and power distribution. The optimization is carried out within a master-slave framework, where the SCA handles the optimization process and the power flow model evaluates the technical outcomes. Case studies on 33- and 69-bus systems reveal that the SCA achieves significant system losses reductions, with improvements of approximately 35.5227% and 35.6331%, respectively. Moreover, the SCA demonstrates computational efficiency, outperforming other methods such as the vortex search algorithm and previous benchmarks. All simulations and validations were conducted using MATLAB 2024a, confirming the SCA's robustness for this application.

Keywords Sine-Cosine Algorithm; Photovoltaic Integration; D-STATCOM Optimization; Power Flow Analysis; Medium-Voltage Distribution Networks

AMS 2010 subject classifications 62J07

DOI:10.19139/soic-2310-5070-2232

1. Introduction

1.1. General context

The global push for the energy transition is vital, as greenhouse gas emissions increasingly threaten the sustainability of life on Earth [1]. Human activities have significantly contributed to what has now been termed the *Anthropocene*, a period characterized by the profound impact of human behavior on natural systems, particularly on climate patterns [2,3]. The primary driver behind these environmental shifts is a heavy reliance on fossil fuels to meet society's growing energy demands [4,5]. Fossil fuels, including coal, oil, and natural gas, are still the prevalent energy sources in transportation, electricity generation, and industrial production, despite their well-documented contribution to global warming and air pollution [6]. The combustion of these fuels releases large amounts of carbon dioxide and other harmful gases into the atmosphere, exacerbating the greenhouse effect and leading to more frequent and severe climate-related disasters [7,8].

In this context, medium-voltage distribution grids, although not direct sources of emissions, play an indirect role in contributing to global warming. In many countries, the electricity delivered through these grids is generated by

*Correspondence to: O. D. Montoya (Email: odmontoyag@udistrital.edu.co). Facultad de Ingeniería, Universidad Distrital Francisco José de Caldas, Bogotá D.C. 110121, Colombia.

ISSN 2310-5070 (online) ISSN 2311-004X (print)

thermal power plants that burn fossil fuels such as coal, natural gas, or diesel [9, 10]. The inefficiencies of energy distribution, coupled with the carbon-intensive nature of generation, result in a system that further accelerates environmental degradation. By focusing on transitioning these grids towards the integration of renewable energy sources, such as solar and wind power, significant strides can be made in reducing the carbon footprint of the electricity sector. This energy transition, if effectively implemented, has the potential to not only decrease the reliance on fossil fuels, but also to enhance energy security and resilience [11]. Furthermore, advancements in grid technology, energy storage, and distributed generation systems will be crucial in achieving this transition, allowing medium-voltage networks to accommodate cleaner energy and operate more efficiently [12].

1.2. Motivation

To help mitigate the adverse effects of fossil fuel consumption, this research focuses on improving the electrical performance of distribution networks from the utility's perspective by optimally integrating renewable energy resources, specifically photovoltaic systems (PVs) and distribution static compensators (D-STATCOMs) [13]. The integration of these distributed energy resources is approached from an economic standpoint, aiming to minimize the operational costs of energy production at the substation level, where conventional energy sources are used [14]. These costs are intrinsically linked to carbon dioxide emissions, as shown by [15]. Integrating PV and D-STATCOM systems into electrical grids poses a significant challenge due to the complexity of the electrical network's equivalent model, which implies a mixed-integer nonlinear programming (MINLP) problem [16]. Given the non-convexity and disjunctive characteristics of the solution space, classical optimization techniques are unable to ensure a global optimum [17]. To address this issue, our research proposes an efficient optimization framework that leverages a master-slave approach, combining a metaheuristic optimization algorithm with classical power flow analysis. The effectiveness of this methodology is demonstrated through numerical results that outperform recent findings in the literature.

1.3. Literature review

The simultaneous integration of PVs and D-STATCOMs has recently garnered attention in the literature, which has explored various optimization approaches – including master-slave methodologies. Below, some of the most relevant works in this area are discussed.

The authors of [13] applied the vortex search algorithm (VSA) to optimally locate and size PVs and D-STATCOMs in electrical networks while aiming to minimize the net present value associated with investment and operating costs over a 20-year period. Numerical results demonstrated the effectiveness of the proposed approach. However, no comparative analysis with other combinatorial optimizers was conducted.

In [18], the generalized normal distribution (GNDO) algorithm was employed to address the placement and sizing of PVs and D-STATCOMs in distribution networks with 33 and 69 nodes. Numerical results confirmed the effectiveness of this methodology, indicating improvements over the VSA approach. Similarly, [11] applied the multi-verse optimization (MVO) algorithm to this problem, with excellent results that surpassed those obtained with the VSA.

The work by [19] introduced a hybrid optimization technique combining analytical and metaheuristic methods to optimally place and size distributed generators and D-STATCOMs in distribution networks. The goal was to minimize total losses and enhance voltage profiles. Key bus parameters were optimized using the particle swarm optimization (PSO) algorithm, while a probabilistic load model was developed via Monte Carlo simulation to account for demand variability. The effectiveness of the proposed approach was validated on a real distribution system from South Kerman, Iran.

The study by [20] presented a method for integrating microgrids and D-STATCOM controllers into power systems in order to enhance voltage profiles, improve system reliability, and reduce power losses in radial distribution networks. This study used PSO to find the optimal MG and D-STATCOM sizes while applying the loss sensitivity factor and the voltage stability index to determine the optimal locations. Simulations conducted in an IEEE 30-bus RDS demonstrated that this strategic placement improved voltage profiles and reduced technical losses, enhancing the overall power quality.

The authors of [21] presented a novel smart PV-STATCOM system, wherein a PV inverter was controlled to function as a STATCOM. This device provided continuous voltage control to meet critical system needs around the clock. At night, the capacity of the inverter was fully utilized for STATCOM operations, while, in the face daytime disturbances, it temporarily suspended real power generation to enhance reactive power support. Once the disturbance was resolved, the solar farm returned to normal power production. The low voltage ride-through capability of the PV-STATCOM was demonstrated through EMTDC/PSCAD simulations and a laboratory implementation with dSPACE control, achieving a response time of 1-2 cycles, comparable to a conventional STATCOM and potentially generating revenue for voltage control services.

In [22], a method for compensating harmonics and zero-sequence components from unbalanced nonlinear loads using a PV-STATCOM was proposed. This approach utilizes a PV generator instead of passive storage components, improving grid power quality without additional costs while implementing instantaneous power and current control strategies. The results showed a total harmonic distortion reduction from 28.80% to 2.03% and a decrease in the zero-sequence component from 31.50% to 4.26%. The PV-STATCOM also exhibited stability, effectively adapting to variable solar radiation and load conditions.

The key aspects of the above-presented literature review are as follows:

1. **Optimization techniques for PV and D-STATCOM placement and sizing**: Multiple studies have focused on finding optimal locations and sizes for PVs and D-STATCOMs in order to minimize costs and losses as well as enhance voltage profiles in distribution networks. Various optimization approaches have been employed, including the VSA, the GNDO algorithm, and MVO, reporting improvements in system performance.
2. **Hybrid analytical and metaheuristic approaches**: Some works have proposed hybrid optimization techniques that combine analytical and metaheuristic methods, such as PSO, alongside probabilistic load modeling via Monte Carlo simulation. These methodologies aim to improve voltage profiles and reduce losses in real distribution systems, with successful validations on standard test feeders and real-world grids.
3. **PV-STATCOMs for enhanced grid quality and stability**: The use of PV-STATCOMs as versatile reactive power compensators has been explored to improve power quality, reduce harmonics, and stabilize voltage in power systems. Innovations include smart inverter PV-STATCOMs capable of providing voltage control during the day and at night, compensating for harmonics, and adapting to solar radiation and load variations effectively, while also achieving notable reductions in total harmonic distortion and improving grid stability.

1.4. Contributions and scope

Considering the above, the primary contribution of this research lies in its master-slave optimization approach to the simultaneous integration of PVs and D-STATCOMs in medium-voltage distribution networks. In the master stage, the sine-cosine algorithm (SCA) is employed as a solution methodology while utilizing a discrete-continuous codification. The discrete part of this codification specifies the optimal locations for installing PVs and D-STATCOMs, while the continuous part determines their nominal sizes. In the slave stage, the successive approximations power flow method is used to ensure the technical feasibility of the solution, with an emphasis on maintaining voltage levels and accurate power injection in the distributed energy resources (DERs) used. Notably, the numerical results presented in this research demonstrate improvements over literature-reported approaches, specifically outperforming the VSA discussed by the authors of [13].

It is worth highlighting that the following aspects were considered within the scope of this research:

i. The electrical configuration of the distribution network, including its daily active and reactive power demand patterns, was provided by the distribution company, based on measurements taken at the substation terminals.
ii. The renewable generation profile was derived by analyzing and filtering historical data on solar resource availability. This process allowed determining the solar generation curve with the highest likelihood of occurrence in the area served by the studied medium-voltage distribution feeder.
iii For the sake of comparison, the VSA reported in [13] was implemented under the same parameter conditions of our proposal.

1.5. Document structure

The remainder of this document is organized as follows. Section 2 outlines the optimization model for the optimal placement and sizing of PVs and D-STATCOMs in distribution networks. This model uses a MINLP approach to minimize the expected investment and operating costs over a 20-year lifespan. Section 3 details the solution methodology, *i.e.*, a hybrid optimization approach combining the SCA with a multi-period optimal power flow problem within a master-slave framework aimed at effectively addressing the siting and sizing of PVs and D-STATCOMs in electrical distribution grids. Section 4 describes the main characteristics of the test feeders used, specifically the 33- and 69-bus grids, as well as the parametrization of objective functions, the grid topology, and the operating constraints. Section 5 presents some computational validations and numerical comparisons with results reported in the literature, along with the corresponding analyses and discussions. Finally, Section 6 provides the main concluding remarks of this work and outlines potential future research directions.

2. PV and D-STATCOM location and sizing model

The task of determining the optimal locations and sizes for PVs and D-STATCOMs is a complex MINLP problem. In this formulation, the continuous variables represent power flow aspects such as voltage and power levels, while the integer variables specify the nodes where the PVs and D-STATCOMs are to be installed. The objective of this model is to plan the integration of these devices in a way that minimizes the overall costs, which include the expected energy purchases from the substation, as well as the investment, operating, and maintenance expenses associated with the PVs and D-STATCOMs [18]. The detailed formulation that represents the studied problem is presented below.

2.1. Objective function

The combined investment, maintenance, and operating costs associated with the simultaneous integration of PV generators and D-STATCOMs in distribution networks can be expressed as shown in (1).

$$\min z_{\text{cost}_1} = z_1 + z_2, \tag{1}$$

where z_1 and z_2 are defined by Equations (2) and (3).

$$z_1 = C_{kWh} T f_a f_c \left(\sum_{h \in H} \sum_{i \in \mathcal{N}} p_{i,h}^{cg} \Delta h \right), \tag{2}$$

$$z_2 = C_{pv} f_a \left(\sum_{i \in \mathcal{N}} p_i^{pv} \right) + T \left(\sum_{h \in H} \sum_{i \in \mathcal{N}} C_{O\&M}^{pv} p_{i,h}^{pv} \Delta h \right) + \gamma \sum_{i \in \mathcal{N}} \left(\omega_1 ({q_i}^{comp})^2 + \omega_2 {q_i}^{comp} + \omega_3 \right) {q_i}^{comp}. \tag{3}$$

In this context, z_1 represents the function that calculates the yearly costs associated with purchasing or producing energy from conventional generators throughout the lifespan of the distributed PVs. In addition, the parameter C_{kWh} denotes the average energy cost at the substation bus, while T signifies the total number of days in a year (365). The variable $p_{i,h}^{cg}$ specifies the active power generation at the slack bus connected to node i at a specific time h, and Δh is the time interval used for representing the operation data for a single day. The function z_2 accounts for the annualized investment and maintenance costs associated with installing PV generation units within the electrical network. Furthermore, C_{pv} stands for the installation cost per unit capacity of the PV plants (USD/kWp), and p_i^{pv} is the capacity of the PV systems installed. The term $C_{O\&M}^{pv}$ indicates the average operating and maintenance expenses of the PV sources. The coefficients ω_1, ω_2, and ω_3 represent the cubic, quadratic, and linear costs associated with the installation of a D-STATCOM at bus i, with a nominal capacity of ${q_i}^{comp}$. The factor γ denotes the annualization rate for investments in reactive power compensators. Finally, $\mathcal{H}$, $\mathcal{N}$, and $\mathcal{T}$ are sets representing the daily periods,

the nodes in the network, and the years analyzed, respectively. The factors f_a and f_c are defined as follows:

$$f_a = \left(\frac{t_a}{1-(1+t_a)^{-N_t}} \right), \tag{4}$$

$$f_c = \sum_{t \in \mathcal{T}} \left(\frac{1+t_e}{1+t_a} \right)^t. \tag{5}$$

In this formulation, f_a is the annualization factor that converts the initial capital costs into the equivalent annual expenses, and f_c represents the projected cumulative costs of energy purchasing over the duration of the project. The parameter t_a denotes the fixed rate of return on investments for the network owner or operator over the planning period, while N_t specifies the project's lifespan in years. Additionally, t_e indicates the anticipated percent increase in energy purchase costs over the 20-year planning horizon, and the set $\mathcal{T}$ contains all the years considered in the planning period.

2.2. Set constraints

Determining the optimal placement and sizing of PVs and D-STATCOMs in electrical distribution networks requires considering a variety of constraints typically related to the active and reactive power balance, voltage regulation limits, and the operational capacities of the devices analyzed, among others. The complete set of constraints is detailed below [18].

$$p_{i,h}^{cg} + p_{i,h}^{pv} - P_{i,h}^{d} = v_{i,h} \sum_{j \in \mathcal{N}} Y_{ij} v_{j,h} \cos(\theta_{i,h} - \theta_{j,h} - \varphi_{ij}), \quad \left\{ \begin{matrix} \forall i \in \mathcal{N} \\ h \in \mathcal{H} \end{matrix} \right\} \tag{6}$$

$$q_{i,h}^{cg} + q_{i,h}^{comp} - Q_{i,h}^{d} = v_{i,h} \sum_{j \in \mathcal{N}} Y_{ij} v_{i,h} \sin(\theta_{i,h} - \theta_{j,h} - \varphi_{ij}), \quad \left\{ \begin{matrix} \forall i \in \mathcal{N} \\ h \in \mathcal{H} \end{matrix} \right\} \tag{7}$$

$$P_i^{cg,\min} \leq p_{i,h}^{cg} \leq P_i^{cg,\max}, \quad \left\{ \begin{matrix} \forall i \in \mathcal{N} \\ h \in \mathcal{H} \end{matrix} \right\} \tag{8}$$

$$Q_i^{cg,\min} \leq q_{i,h}^{cg} \leq Q_i^{cg,\max}, \quad \left\{ \begin{matrix} \forall i \in \mathcal{N} \\ h \in \mathcal{H} \end{matrix} \right\} \tag{9}$$

$$x_i^{pv} P_{i,h}^{pv,\min} \leq p_i^{pv} \leq x_i^{pv} P_{i,h}^{pv,\max}, \quad \left\{ \begin{matrix} \forall i \in \mathcal{N} \\ h \in \mathcal{H} \end{matrix} \right\} \tag{10}$$

$$p_{i,h}^{pv} = G_{i,h}^{pv} p_i^{pv}, \quad \left\{ \begin{matrix} \forall i \in \mathcal{N} \\ h \in \mathcal{H} \end{matrix} \right\} \tag{11}$$

$$v^{\min} \leq v_{i,h} \leq v^{\max}, \quad \left\{ \begin{matrix} \forall i \in \mathcal{N} \\ h \in \mathcal{H} \end{matrix} \right\} \tag{12}$$

$$\sum_{i \in \mathcal{N}} x_i^{pv} \leq N_{pv}^{ava} \tag{13}$$

$$x_i^{comp} Q_i^{comp,\min} \leq q_i^{comp} \leq x_i^{comp} Q_{i,h}^{comp,\max}, \quad \{\forall i \in \mathcal{N}\} \tag{14}$$

$$q_{i,h}^{comp} = q_i^{comp}, \quad \{\forall i \in \mathcal{N}\} \tag{15}$$

$$\sum_{i \in \mathcal{N}} x_i^{comp} \leq N_{comp}^{ava}, \tag{16}$$

In this model, Equation (6) specifies the active power balance, where $P_{i,h}^{d}$ denotes the active power demand at node i and time h. The voltage magnitudes at nodes i and j at time h are given by $V_{i,h}$ and $V_{j,h}$, with their respective angles $\theta_{i,h}$ and $\theta_{j,h}$. The components Y_{ij} and φ_{ij} represent the magnitude and angle of the admittance matrix between nodes i and j. Equation (7) defines the reactive power balance for each node and time period, where

$Q^{d}_{i,h}$ is the reactive power demand at node i, $q^{cg}_{i,h}$ is the reactive power provided by the conventional generator at node i, and $q^{comp}_{i,h}$ represents the reactive power injected by a D-STATCOM at bus i, all during period h.

Equation (8) establishes the bounds for active power generation by conventional sources, as denoted by the parameters $P^{cg,\min}_{i}$ and $P^{cg,\max}_{i}$. Similarly, Equation (9) sets the reactive power limits for the conventional generator at node i, which are signified by $Q^{cg,\min}_{i}$ and $Q^{cg,\max}_{i}$. The Inequality Constraint (10) specifies the active power generation bounds for the PVs at node i and time h, given as $P^{pv,\min}_{i,h}$ and $P^{pv,\max}_{i,h}$. These are enforced when the binary variable x^{pv}_{i} equals 1. Equation (11) ensures that the PV generators operate at their maximum power availability, adhering to the generation curve $G^{pv}_{i,h}$.

Across all nodes and periods, voltage regulation is governed by Inequality Constraint (12), with the permissible voltage range defined by $v^{\min}$ and $v^{\max}$. Constraint (13) limits the total number of PVs that can be installed across the distribution network, denoted by N^{ava}_{pv}. Box Constraint (14) defines the reactive power capacity limits of a D-STATCOM connected to bus i, which are represented by $Q^{comp,\min}_{i}$ and $Q^{comp,\max}_{i}$, while the binary variable x^{comp}_{i} indicates whether the D-STATCOM is installed. Equality Constraint (15) mandates that the D-STATCOM must operate at full dispatch during each period, with $q^{comp}_{i,h}$ representing its hourly reactive power dispatch. Lastly, Inequality Constraint (16) sets the maximum number of D-STATCOMs that can be installed in the network, as given by N^{ava}_{comp}.

2.3. Model characteristics

To highlight the complexities inherent in the MINLP model for the studied problem, its structure can be categorized into three main groups: non-convex, convex, and binary characteristics.

i. **Non-convex characteristics:** The Objective Function (1), along with Equality Constraints (6) and (7), exhibits a nonlinear and non-convex behavior. This is primarily due to the use of trigonometric sine and cosine terms, to the interactions between voltage variables, and to cubic expressions.
ii. **Convex characteristics:** The set of constraints encompassing Inequalities (8), (9), and (12), together with the equalities in (11) and (15), exhibit a linear and convex structure. Most of these constraints define the upper and lower bounds of the decision variables.
iii. **Binary:** Inequalities (10), (13), (14), and (16) fall into the binary category as they involve discrete decision variables, governing conditions on whether certain actions are taken within the model.

It is important to note that Equations (4) and (5) are not included in this classification, since they provide constant parameters associated with annualization and projected energy costs over the project's duration.

3. Solution methodology

The optimization model represented by Equations (1)–(16) is solved by implementing a two-stage approach. The SCA is applied in the master stage, while a power flow method is used in the slave stage, with the former being responsible for determining the optimal placement and sizing of the PVs and D-STATCOMs. Once these variables have been established, they are entrusted to the slave stage, where a power flow algorithm for distribution networks evaluates the power balance constraints. This algorithm provides an analysis of the voltage levels and power generation for each scenario. The key components of this solution methodology are detailed below.

3.1. Fitness function

Fitness functions are widely used in metaheuristic optimization for dealing with model constraints via penalty factors [23]. A fitness function (*i.e.*, F_f) for the problem regarding the sizing and location of PVs and D-STATCOMs is defined in (17).

$$F_f = z + \sum_{k\in\mathbb{C}} \alpha_k(x). \tag{17}$$

The term $\alpha_k(x)$ represents the penalty function applied to the objective function when the k^{th} constraint is violated, with **C** being the set of all constraints considered within the fitness function. To define the specific form of each $\alpha_k(x)$, it is important to consider the following: (i) the power balance constraint from the slave stage is excluded from the penalty process, as it is resolved within it (see Equations (6) and (7)); (ii) the constraints related to the location and sizing of PVs and D-STATCOMs are inherently enforced through the encoding method; and (iii) only operational constraints such as the slack generation limits (Equations (8) and (9)) and the voltage regulation bounds (Equation (12)), among others, are included in the penalty term of the fitness function in Equation (17).

3.2. Slave stage: multi-period power flow solution

To evaluate each potential solution offered by the master stage (*i.e.*, the SCA), a power flow tool is required, which, in the case of this work, is based on the successive approximations method. This tool is essential for solving the nonlinear equality constraint associated with the power balances. Using a complex variable representation, the power flow tool leverages a numerical approach to compute all voltage profiles in Equations (6) and (7). It presupposes that the power inputs and outputs are fixed. The recursive power flow equation for the successive approximations method is presented in Equation (18), as described in [18].

$$\mathbb{V}_{d,h}^{t+1} = -\mathbb{Y}_{d,d}^{-1}\left[\text{diag}^{-1}\left(\mathbb{V}_{d,h}^{t,\star}\right)\mathbb{S}_{d,h}^{\star} - \mathbb{Y}_{d,g}\mathbb{V}_{g,h}\right], \tag{18}$$

In this context, $\mathbb{V}_{d,h}^{t+1}$ represents a vector that includes all the voltages at the demand nodes for period h during iteration $t+1$. The matrix $\mathbb{Y}_{d,d}^{-1}$ denotes the inverse of the complex nodal admittance matrix, which defines the relationships between demand nodes. The vector $\mathbb{S}_{d,h}^{\star}$ captures the power demanded by the constant power loads, as well as the power injected by the PV plants and D-STATCOMs, specifically defined as $\mathbb{S}_{d,h} = \mathbb{S}_{d,h}^{dg} + \mathbb{S}_{DERs,h}^{b} - \mathbb{S}_{d,h}^{d}$. Furthermore, $\mathbb{Y}_{d,g}$ is a rectangular matrix linking the slack node (*i.e.*, the conventional source node) to the demand nodes. Finally, $\mathbb{V}_{g,h}$ represents the slack voltage, which is well-known in power flow analysis, as it corresponds to the substation's nominal voltage level.

It is important to highlight that the recursive formula in Equation (18) reaches convergence once the stopping criterion in Equation (19) is fulfilled, where ε is set to a value of 1×10^{-10} [23].

$$\max_{h}\left|\mathbb{V}_{d,h}^{t+1} - \mathbb{V}_{d,h}^{t}\right| \leq \varepsilon, \ \{h \in \mathbf{H}\} \tag{19}$$

Upon meeting the criterion specified in Equation (19), the power flow formula in Equation (18) is deemed to have converged. Subsequently, the power produced by the conventional source for each period h is calculated according to Equation (20) [24].

$$\mathbb{S}_{g,h} = \mathbb{Y}_{d,g}\mathbb{V}_{g,h} + \mathbb{Y}_{g,d}\mathbb{V}_{d,h}. \ \{h \in \mathbf{H}\} \tag{20}$$

Here, $\mathbb{S}_{g,h}$ denotes the vector corresponding to the power injected by the conventional source at time h.

3.3. Master stage: the sine-cosine algorithm

The SCA is a metaheuristic optimization method belonging to the family of mathematics-inspired algorithms, which explores and exploits the solution space by employing trigonometric functions [25]. This approach is particularly well-suited for addressing power coordination issues in battery systems, as it can deal with continuous optimization problems. The SCA was originally introduced by [25] to tackle the optimal power flow problem in transmission systems, which implies a large-scale and complex nonlinear (continuous) optimization model.

3.3.1. Problem codification and initial population For the studied problem, the decision variables correspond to the optimal siting and sizing of PVs and D-STATCOMs in electric distribution grids. An example of the proposed

codification, which considers two PV generators and two D-STATCOMs in a distribution network with 33 nodes and maximum sizes of 1800 MW and 1500 kvar, is presented below [18].

$$x_j = \begin{bmatrix} 14 & 21 & 8 & 30 & 989.41 & 1206.87 & 469.32 & 995.87 \end{bmatrix}, \tag{21}$$

which means the following:

i. The PV sources are located at buses 14 and 25, with nominal sizes of 989.41 kW and 1206.87 kW, respectively.
ii. The D-STATCOMs are located at nodes 8 and 30, with nominal sizes of 469.32 kvar and 995.87 kvar.

In the proposed encoding (Equation (21)), x_j represents the j^{th} potential solution in the population at iteration p (*i.e.*, X^p). The matrix X^p has dimensions of $n_s \times n_v$, where n_v denotes the number of decision variables and n_s indicates the number of possible solutions.

It is important to note that, in order to generate each x_j^p (where $p = 0$), the rule described in Equation (22) is applied:

$$x_{j,l} = x_l^{\min} + \beta_l \left(x_l^{\max} - x_l^{\min} \right), \ \begin{Bmatrix} l = 1, 2, ..., n_v \\ j = 1, 2, ..., n_s \end{Bmatrix} \tag{22}$$

where β_l is a random value uniformly distributed within the interval [0, 1], and $x_l^{\min}$ and $x_l^{\max}$ are the lower and upper bounds of the decision variables, respectively.

3.3.2. Evolution rules After creating the initial population X^p at iteration $p = 0$, the next task is to identify the optimal solution within it, denoted as x_{best}^p.

To find the best solution for a given iteration p, all n_s candidate solutions in the population X^p are evaluated based on the objective function or the fitness function. The latter is used as follows to determine the optimal solution:

$$x_{\text{best}}^p = \left\{ x_j^p \mid x_j^p \to \min \left(F_f \left(x_j^p \right) \right), \ \forall j = 1, 2, ..., n_s \right\}, \tag{23}$$

where x_j^p is the j^{th} solution in the population at iteration p, and $F_f \left(x_j^p \right)$ denotes the fitness function evaluated for the solution x_j^p (see Equation (17)).

Once the best solution of the current iteration has been identified, the update rule presented in Equation (24) is applied to all solutions, $\forall k = 1, 2, ..., n_s$:

$$y_j^t = \begin{cases} x_j^p + r_1 \sin\left(r_2\right) \cdot \left| r_3 x_{\text{best}}^p - x_j^p \right| & r_4 \leq \frac{1}{2} \\ x_j^p + r_1 \cos\left(r_2\right) \cdot \left| r_3 x_{\text{best}}^p - x_j^p \right| & r_4 > \frac{1}{2} \end{cases}. \tag{24}$$

In this equation, y_j^p is the candidate solution for the subsequent iteration; r_1 represents a linear decay function; r_2 is a vector of random variables uniformly distributed in $[0, 2\pi]$, with dimensions of $1 \times n_v$; and r_3 and r_4 are random values uniformly distributed between 0 and 1. It is also important to note that $v \cdot w$ represents the element-wise product between the vectors v and w. The parameter r_1 is computed at each iteration as follows:

$$r_1 = a \left(1 - \frac{p}{p_{\max}} \right), \tag{25}$$

where $p_{\max}$ is the total number of iterations and a is a scaling factor defined by the user, typically set to $a = 2$, as suggested by [25].

Each potential solution y_k^p is then checked to ensure that it remains within the bounds set for the decision variables. The correction rule to be applied to each variable, for all $\forall j = 1, 2, ..., n_v$ and $\forall l = 1, 2, ..., n_s$, is provided in Equation (26):

$$y_{j,l}^p = \begin{cases} y_{j,l} & \text{if } x_l^{\min} \leq y_{j,l} \leq x_l^{\max} \\ x_l^{\min} & \text{if } y_{j,l} < x_l^{\min} \\ x_l^{\max} & \text{if } y_{j,l} > x_l^{\max} \end{cases}. \tag{26}$$

This rule ensures that any solution outside the specified bounds is corrected to the nearest limit.

3.3.3. Population replacement After generating the new candidate solutions, denoted as y_k^p, it is necessary to decide whether these solutions will be included in the population for the next iteration. To this effect, the performance function value $F_f\left(y_j^p\right)$ must be evaluated. Based on this value, the replacement rule for the population is defined:

$$x_j^{p+1} = \begin{cases} y_j^p, & F_f\left(y_j^p\right) < F_f\left(x_j^p\right) \\ x_j^p, & F_f\left(y_j^p\right) \geq F_f\left(x_j^p\right) \end{cases}, \quad \forall j = 1, 2, ..., n_s. \tag{27}$$

This rule allows updating the population by replacing the existing solutions with new candidates if they perform better according to the fitness function.

3.3.4. Stopping criteria In the context of metaheuristic optimization techniques, since solutions are progressively approximated through sequential programming, two commonly used stopping criteria can be found in the literature. First, the search and optimization process may conclude (i) once the maximum number of iterations set by the user has been reached, or (ii) when no improvements are observed in the performance function over a period of $k_{\max}$ consecutive iterations.

For the second criterion, a counter is typically implemented, which tracks the iterations with no improvement in the objective function. If this stopping rule is applied, the value of $k_{\max}$ is set by the user. The generally recommended is between 10% and 30% of the total iteration count.

4. Test feeders and model characterization

Our hybrid master-slave optimization approach, which combines the SCA and the successive approximations power flow method for the optimal siting and sizing of PVs and D-STATCOMs in distribution networks, was validated using the standard 33- and 69-bus test feeders [18]. Figure 1 illustrates the electrical configuration of both systems, while their corresponding electrical parameters are presented in Table 1. These feeders maintain a radial topology and are designed to operate with a nominal voltage of 12,660 V at the substation terminals. Moreover, the permissible voltage variations for these systems are constrained to $\pm 10\%$ [11].

The effectiveness of the proposed method was evaluated while considering the expected active and reactive power demand curves (profiles) as well as the average solar power availability [13]. These curves are illustrated in Figure 2.

To calculate the values of the objective function, the parameters provided in Table 2 were used for the PV generation sources. In addition, the cost details related to the D-STATCOMs are outlined in Table 3.

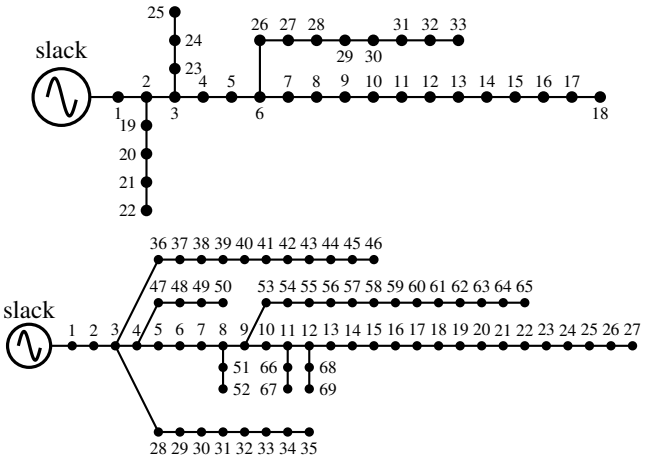

Figure 1. Single-phase diagrams of the 33- and 69-bus systems

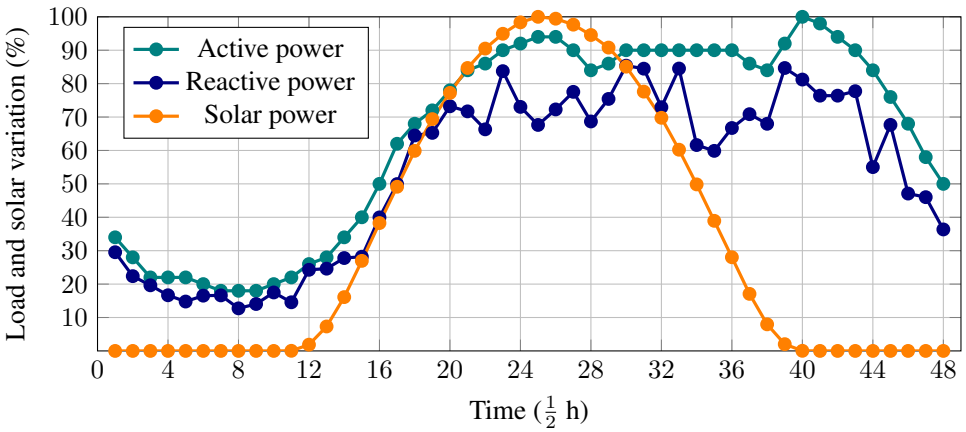

Figure 2. Daily behavior of power consumption and solar generation

5. Numerical validations

The computational implementation of the proposed master-slave optimization approach was carried out using MATLAB (version 2024a) on a PC equipped with an AMD Ryzen 7 3700 processor (2.3 GHz), 16 GB of RAM, and a 64-bit version of Microsoft Windows 10 Single Language. Custom scripts were developed for both the SCA and the successive approximations power flow method. To evaluate the effectiveness of our approach, a comparative analysis against the VSA technique reported in [13] was conducted. Each algorithm was configured to deploy PV sources with a maximum capacity of 2400 kW and D-STATCOMs with a rated capacity of up to 2000 kvar, thus allowing for a maximum of three PVs and three D-STATCOMs. The population size for all algorithms was set to 50 individuals over 1000 iterations. Furthermore, 100 consecutive repetitions were conducted to accurately assess the solution methodologies from a statistical standpoint.

5.1. Results for the 33-bus grid

Table 4 compares the numerical results obtained for the 33-bus grid.

These results show that:

Table 1. Branch and load data for the 33- and 69-bus grids

The 33-bus grid											
Node i	**Node j**	**R_{ij} (Ω)**	**X_{ij} (Ω)**	**P_j (kW)**	**Q_j (kvar)**	**Node i**	**Node j**	**R_{ij} (Ω)**	**X_{ij} (Ω)**	**P_j (kW)**	**Q_j (kvar)**
1	2	0.0922	0.0477	100	60	17	18	0.7320	0.5740	90	40
2	3	0.4930	0.2511	90	40	2	19	0.1640	0.1565	90	40
3	4	0.3660	0.1864	120	80	19	20	1.5042	1.3554	90	40
4	5	0.3811	0.1941	60	30	20	21	0.4095	0.4784	90	40
5	6	0.8190	0.7070	60	20	21	22	0.7089	0.9373	90	40
6	7	0.1872	0.6188	200	100	3	23	0.4512	0.3083	90	50
7	8	1.7114	1.2351	200	100	23	24	0.8980	0.7091	420	200
8	9	1.0300	0.7400	60	20	24	25	0.8960	0.7011	420	200
9	10	1.0400	0.7400	60	20	6	26	0.2030	0.1034	60	25
10	11	0.1966	0.0650	45	30	26	27	0.2842	0.1447	60	25
11	12	0.3744	0.1238	60	35	27	28	1.0590	0.9337	60	20
12	13	1.4680	1.1550	60	35	28	29	0.8042	0.7006	120	70
13	14	0.5416	0.7129	120	80	29	30	0.5075	0.2585	200	600
14	15	0.5910	0.5260	60	10	30	31	0.9744	0.9630	150	70
15	16	0.7463	0.5450	60	20	31	32	0.3105	0.3619	210	100
16	17	1.2860	1.7210	60	20	32	33	0.3410	0.5302	60	40
The 69-bus grid											
Node i	**Node j**	**R_{ij} (Ω)**	**X_{ij} (Ω)**	**P_j (kW)**	**Q_j (kvar)**	**Node i**	**Node j**	**R_{ij} (Ω)**	**X_{ij} (Ω)**	**P_j (kW)**	**Q_j (kvar)**
1	2	0.0005	0.0012	0.00	0.00	3	36	0.0044	0.0108	26.00	18.55
2	3	0.0005	0.0012	0.00	0.00	36	37	0.0640	0.1565	26.00	18.55
3	4	0.0015	0.0036	0.00	0.00	37	38	0.1053	0.1230	0.00	0.00
4	5	0.0251	0.0294	0.00	0.00	38	39	0.0304	0.0355	24.00	17.00
5	6	0.3660	0.1864	2.60	2.20	39	40	0.0018	0.0021	24.00	17.00
6	7	0.3810	0.1941	40.40	30.00	40	41	0.7283	0.8509	1.20	1.00
7	8	0.0922	0.0470	75.00	54.00	41	42	0.3100	0.3623	0.00	0.00
8	9	0.0493	0.0251	30.00	22.00	42	43	0.0410	0.0478	6.00	4.30
9	10	0.8190	0.2707	28.00	19.00	43	44	0.0092	0.0116	0.00	0.00
10	11	0.1872	0.0619	145.00	104.00	44	45	0.1089	0.1373	39.22	26.30
11	12	0.7114	0.2351	145.00	104.00	45	46	0.0009	0.0012	29.22	26.30
12	13	1.0300	0.3400	8.00	5.00	4	47	0.0034	0.0084	0.00	0.00
13	14	1.0440	0.3450	8.00	5.50	47	48	0.0851	0.2083	79.00	56.40
14	15	1.0580	0.3496	0.00	0.00	48	49	0.2898	0.7091	384.70	274.50
15	16	0.1966	0.0650	45.50	30.00	49	50	0.0822	0.2011	384.70	274.50
16	17	0.3744	0.1238	60.00	35.00	8	51	0.0928	0.0473	40.50	28.30
17	18	0.0047	0.0016	60.00	35.00	51	52	0.3319	0.1114	3.60	2.70
18	19	0.3276	0.1083	0.00	0.00	9	53	0.1740	0.0886	4.35	3.50
19	20	0.2106	0.0690	1.00	0.60	53	54	0.2030	0.1034	26.40	19.00
20	21	0.3416	0.1129	114.00	81.00	54	55	0.2842	0.1447	24.00	17.20
21	22	0.0140	0.0046	5.00	3.50	55	56	0.2813	0.1433	0.00	0.00
22	23	0.1591	0.0526	0.00	0.00	56	57	1.5900	0.5337	0.00	0.00
23	24	0.3463	0.1145	28.00	20.00	57	58	0.7837	0.2630	0.00	0.00
24	25	0.7488	0.2475	0.00	0.00	58	59	0.3042	0.1006	100.00	72.00
25	26	0.3089	0.1021	14.00	10.00	59	60	0.3861	0.1172	0.00	0.00
26	27	0.1732	0.0572	14.00	10.00	60	61	0.5075	0.2585	1244.00	888.00
3	28	0.0044	0.0108	26.00	18.60	61	62	0.0974	0.0496	32.00	23.00
28	29	0.0640	0.1565	26.00	18.60	62	63	0.1450	0.0738	0.00	0.00
29	30	0.3978	0.1315	0.00	0.00	63	64	0.7105	0.3619	227.00	162.00
30	31	0.0702	0.0232	0.00	0.00	64	65	1.0410	0.5302	59.00	42.00
31	32	0.3510	0.1160	0.00	0.00	11	66	0.2012	0.0611	18.00	13.00
32	33	0.8390	0.2816	14.00	10.00	66	67	0.0470	0.0140	18.00	13.00
33	34	1.7080	0.5646	19.50	14.00	12	68	0.7394	0.2444	28.00	20.00
34	35	1.4740	0.4873	6.00	4.00	68	69	0.0047	0.0016	28.00	20.00

Table 2. Model parameters associated with the optimal placement and sizing of PV plants in distribution grids

Parameter	**Value**	**Unit**	**Parameter**	**Value**	**Unit**
C_{kWh}	0.1390	USD/kWh	T	365	days
t_a	10	%	N_t	20	years
Δh	1	h	t_e	2	%
C_{pv}	1036.49	USD/kWp	C_{0andM}	0.0019	USD/kWh
N_{pv}^{ava}	3	-	$p_i^{pv,\max}$	2400	kW
$P_k^{pv,\min}$	0	kW			

Table 3. Objective function parameters (z)

Par.	Value	Unit	Par.	Value	Unit
ω_1	0.30	USD/Mvar^3	ω_2	-305.10	USD/Mvar^2
ω_3	127,380	USD/Mvar	γ	1/20	—
$Q_i^{comp,\min}$	0	Mvar	$Q_{i,h}^{comp,\max}$	2000	kvar
$P_i^{cg,\min}$	0	W	$P_i^{cg,\max}$	5000	kW
$Q_i^{cg,\min}$	0	var	$Q_i^{cg,\max}$	5000	kvar

Table 4. Numerical results obtained for the 33-bus grid

Scen.	x_i^{comp} (Node)	q_i^{comp} (Mvar)	x_i^{pv} (Node)	p_i^{pv} (MW)	A_{cost_3} (USD)	Ave. time (s)
Benchmark case	—	—	—	—	3,553,557.38	—
VSA	[6, 15, 31]	[0.3801, 0.0640, 0.3543]	[9, 14, 31]	[0.9844, 0.6312, 1.7602]	2,292,022.62	305.36
SCA	[11, 12, 30]	[0.0092, 0.1143, 0.4617]	[7, 14, 31]	[0.4348, 1.8842, 1.0836]	2,291,234.65	305.97

i. The optimization algorithms reported reductions ranging from 35.5006% to 35.5227% in the objective function value. This corresponds to net profit figures of approximately $1,261,534.76$ USD for the VSA and $1,262,322.73$ USD for the SCA. Note that the SCA outperformed the VSA by providing additional savings of roughly 787.97 USD. This improvement suggests that the SCA can achieve more effective cost reductions and enhance profitability in comparison with the best outcome produced by the VSA.
ii. Regarding the siting of PV sources, both the VSA and SCA consistently identified bus 31 as the most suitable location for renewable generation sources. The optimal sizes for PV installation at this bus ranged between 1083.6 kW and 1706.2 kW, showcasing its potential for efficient energy generation (the same analysis applies to node 14). However, no clear trend or preferred placement was observed in relation to the D-STATCOMs across the studied optimization methods, indicating a more variable or case-dependent solution for their sizing and siting.

The optimal solution obtained by the SCA reveals that, in order to effectively minimize the expected project costs, approximately 585.20 kvar of reactive power and 3402.60 kWp of active power are required. In contrast, the VSA necessitates 798.40 kvar of reactive power and 3375.80 kWp of active power. These findings suggest that, in the 33-bus feeder, 585.20-798.40 kvar of reactive power and 3375.80-3402.60 kWp of active power are sufficient for minimizing the economic objective function under study.

This comparison between the SCA and the VSA highlights the efficiency of the former in reducing the reactive power requirements to achieve a similar or slightly better cost minimization in comparison with the latter. It also emphasizes that both optimization methods converge on a similar active power capacity range, demonstrating that the requirements are consistent across different algorithms for this specific grid configuration. Overall, the results validate the effectiveness of the analyzed optimization strategies in addressing cost minimization while ensuring that the power requirements remain manageable and within feasible ranges for the 33-bus system.

5.2. Results for the 69-bus grid

Table 5 presents a comparison of the numerical results obtained for the 69-bus feeder.

Table 5. Numerical results obtained for the 69-bus grid

Scen.	x_i^{comp} (Node)	q_i^{comp} (Mvar)	x_i^{pv} (Node)	p_i^{pv} (MW)	A_{cost_3} (USD)	Ave. time (s)
Benchmark case	—	—	—	—	3,723,529.52	—
VSA	[19, 53, 63]	[0.0871, 0.0075, 0.4555]	[15, 33, 62]	[0.8753, 0.5941, 2.0184]	2,400,490.65	1680.10
SCA	[7, 61, 65]	[0.0337, 0.3992, 0.1076]	[18, 59, 61]	[0.8761, 0.3407, 2.2949]	2,396,720.37	1611.16

These numerical results show that:

i. During the project planning period, the SCA significantly outperformed the VSA, with reductions of about 35.6331% in the objective function value. These reductions translate to approximately 3770.28 USD in

savings with respect to the VSA, highlighting the effectiveness of the SCA in achieving lower final objective function values.

ii. In this grid, the VSA achieved a final objective function value of approximately $2,396,720.37$ USD, which represents a reduction of around 35.5318% compared to the benchmark case. The SCA further improved this by about 3770.27 USD, confirming that the SCA method is the most efficient approach for this grid. In terms of processing times, all methods converged to a solution within 1611.16-1680.10 s. Notably, our proposal proved to be the fastest, requiring only around 26.85 minutes, while the VSA was the slowest, with an average processing time of approximately 28 minutes.

It is noteworthy that the optimal solution provided by the proposed SCA requires approximately 540.50 kvar and 3511.70 kWp, while the VSA needs around 550.1 kvar and 3487.80 kWp. These results indicate that, in order to achieve minimized operating costs in the 69-bus grid, reactive power injections should amount to 540.50-550.1 kvar, and active power injections should range from 3487.80 kWp to 3511.70 kWp.

6. Conclusions and future work

This research presented a hybrid optimization approach based on the combination between the SCA and the multi-period successive approximations power flow approach in order to define the optimal sizes and locations of PVs and D-STATCOMs in distribution networks. The analysis of the numerical results leads to the following conclusions:

1. The results for both the 33- and 69-bus grids show that the proposed SCA consistently outperformed the VSA in reducing the objective function value. Specifically, in the 33-bus grid, the SCA achieved additional cost savings of approximately 787.97 USD, and, in the 69-bus grid, it further reduced costs by around 3770.27 USD. These findings demonstrate the higher efficiency of the SCA, achieving reductions of over 35% in operating costs, which translates to substantial economic benefits.
2. In both grids, certain nodes were consistently identified as optimal for renewable generation, particularly node 31 in the 33-bus grid and nodes 18, 59, and 61 in the 69-bus feeder. The active power injections needed to achieve optimal performance were also consistent, with the SCA requiring between 1083.6 kW and 3511.70 kWp in the two grids. On the other hand, the reactive power requirements were lower for the SCA, confirming that it not only optimizes costs but also efficiently sizes the necessary resources for both reactive and active power injection, leading to more feasible and effective solutions.
3. The SCA reported faster processing times in finding optimal solutions when compared to the VSA in both grids. In the 33-bus grid, the methods converged within approximately 305 seconds, while, in the 69-bus grid, the SCA found solutions in around 26.85 minutes, slightly faster than the VSA's average time (about 28 minutes). This efficiency regarding computation times indicates that the SCA is not only better at reducing costs but also more time-efficient, making it a preferable choice for practical implementation.

Future research could focus on the implementation of hybrid optimization techniques to enhance the performance of both the SCA and the VSA in distribution grid applications. Additionally, exploring the integration of stochastic models to account for the variability of renewable energy sources could improve the robustness of the optimization approach. Finally, expanding the analysis to larger-scale grids or multi-objective scenarios could provide further insights into the scalability and versatility of our proposal.

Acknowledgements

The first author would like to express gratitude to Oficina de Investigaciones at Universidad Distrital Francisco José de Caldas for supporting the internal research project with code 33787724, titled "**Desarrollo de una metodología de gestión eficiente de potencia reactiva en sistemas de distribución de media tensión empleando modelos de programación no lineal**."

REFERENCES

1. Sadegh Seddighi, Edward J. Anthony, Hamed Seddighi, and Filip Johnsson. The interplay between energy technologies and human health: Implications for energy transition. *Energy Reports*, 9:5592–5611, December 2023.
2. Michael R Raupach and Josep G Canadell. Carbon and the anthropocene. *Current Opinion in Environmental Sustainability*, 2(4):210–218, October 2010.
3. Shilu Tong, Hilary Bambrick, Paul J. Beggs, Lanming Chen, Yabin Hu, Wenjun Ma, Will Steffen, and Jianguo Tan. Current and future threats to human health in the Anthropocene. *Environment International*, 158:106892, January 2022.
4. Sidhartha Harichandan, Sanjay Kumar Kar, Rohit Bansal, Saroj Kumar Mishra, Marriyappan Sivagnanam Balathanigaimani, and Manoranjan Dash. Energy transition research: A bibliometric mapping of current findings and direction for future research. *Cleaner Production Letters*, 3:100026, December 2022.
5. Sanja Potrč, Lidija Čuček, Mariano Martin, and Zdravko Kravanja. Sustainable renewable energy supply networks optimization – the gradual transition to a renewable energy system within the european union by 2050. *Renewable and Sustainable Energy Reviews*, 146:111186, August 2021.
6. Alice J. Friedemann. *Life after Fossil Fuels: A Reality Check on Alternative Energy*. Springer International Publishing, 2021.
7. Bernard Njindan Iyke. Climate change, energy security risk, and clean energy investment. *Energy Economics*, 129:107225, January 2024.
8. Lamiaa Abdallah and Tarek El-Shennawy. Reducing carbon dioxide emissions from electricity sector using smart electric grid applications. *Journal of Engineering*, 2013:1–8, 2013.
9. Angel D. Ramirez, Beatriz Rivela, Andrea Boero, and Ana M. Melendres. Lights and shadows of the environmental impacts of fossil-based electricity generation technologies: A contribution based on the ecuadorian experience. *Energy Policy*, 125:467–477, February 2019.
10. Talha Bin Nadeem, Mubashir Siddiqui, Muhammad Khalid, and Muhammad Asif. Distributed energy systems: A review of classification, technologies, applications, and policies. *Energy Strategy Reviews*, 48:101096, July 2023.
11. Luis Fernando Grisales-Noreña, Daniel Sanin-Villa, and Oscar Danilo Montoya. Optimal integration of pv generators and d-statcoms into the electrical distribution system to reduce the annual investment and operational cost: A multiverse optimization algorithm and matrix power flow approach. *e-Prime - Advances in Electrical Engineering, Electronics and Energy*, 9:100747, September 2024.
12. Reza Dashti and Mojtaba Rouhandeh. Power distribution system planning framework (a comprehensive review). *Energy Strategy Reviews*, 50:101256, November 2023.
13. Adriana Rincón-Miranda, Giselle Viviana Gantiva-Mora, and Oscar Danilo Montoya. Simultaneous integration of d-statcoms and pv sources in distribution networks to reduce annual investment and operating costs. *Computation*, 11(7):145, July 2023.
14. Juan Caballero-Peña, Cristian Cadena-Zarate, Alejandro Parrado-Duque, and German Osma-Pinto. Distributed energy resources on distribution networks: A systematic review of modelling, simulation, metrics, and impacts. *International Journal of Electrical Power &; Energy Systems*, 138:107900, June 2022.
15. Xuejun Li, Jiaxin Qian, Changhai Yang, Boyang Chen, Xiang Wang, and Zongnan Jiang. New power system planning and evolution path with multi-flexibility resource coordination. *Energies*, 17(1):273, January 2024.
16. Sandeep Kaur, Ganesh Kumbhar, and Jaydev Sharma. A minlp technique for optimal placement of multiple dg units in distribution systems. *International Journal of Electrical Power &; Energy Systems*, 63:609–617, December 2014.
17. Walter Gil-González. Optimal placement and sizing of d-statcoms in electrical distribution networks using a stochastic mixed-integer convex model. *Electronics*, 12(7):1565, March 2023.
18. Oscar Danilo Montoya, Walter Gil-González, and Luis Fernando Grisales-Noreña. Optimal planning of photovoltaic and distribution static compensators in medium-voltage networks via the gndo approach. *Results in Engineering*, 23:102764, September 2024.
19. Farzin Fardinfar and Mostafa Jafari Kermani Pour. Optimal placement of d-statcom and pv solar in distribution system using probabilistic load models. In *2023 10th Iranian Conference on Renewable Energy &; Distributed Generation (ICREDG)*. IEEE, March 2023.
20. Mezigebu Getinet Yenealem. Optimum Allocation of Microgrid and D-STATCOM in Radial Distribution System for Voltage Profile Enhancement Using Particle Swarm Optimization. *International Journal of Photoenergy*, 2024(1), January 2024.
21. Rajiv K. Varma and Ehsan M. Siavashi. Pv-statcom: A new smart inverter for voltage control in distribution systems. *IEEE Transactions on Sustainable Energy*, 9(4):1681–1691, October 2018.
22. Youssef Ait El Kadi, Fatima Zahra Baghli, and Yassine Lakhal. Pv-statcom in photovoltaic systems under variable solar radiation and variable unbalanced nonlinear loads. *International Journal of Electrical and Electronic Engineering &; Telecommunications*, pages 36–48, 2021.
23. Oscar Danilo Montoya, Walter Gil-González, Rubén Iván Bolaños, Diego Fernando Muñoz-Torres, Jesús C. Hernández, and Luis Fernando Grisales-Noreña. Effective power coordination of besus in distribution grids via the sine-cosine algorithm. In *2024 IEEE Green Technologies Conference (GreenTech)*. IEEE, April 2024.
24. Oscar Danilo Montoya and Walter Gil-González. On the numerical analysis based on successive approximations for power flow problems in ac distribution systems. *Electric Power Systems Research*, 187:106454, October 2020.
25. Seyedali Mirjalili. SCA: A Sine Cosine Algorithm for solving optimization problems. *Knowledge-Based Systems*, 96:120–133, March 2016.